THE ASTROPHYSICAL JOURNAL, 398:L41–L44, 1992 October 10

IMAGING OF FOUR PLANETARY NEBULAE IN THE MAGELLANIC CLOUDS USING THE *HUBBLE SPACE TELESCOPE* FAINT OBJECT CAMERA[1]

J. C. BLADES,[2,3] M. J. BARLOW,[4] R. ALBRECHT,[2,5,6,7] C. BARBIERI,[2,8] A. BOKSENBERG,[2,9] P. CRANE,[2,7] J. M. DEHARVENG,[2,10] M. J. DISNEY,[2,11] P. JAKOBSEN,[2,12] T. M. KAMPERMAN,[2,13] I. R. KING,[2,14] F. MACCHETTO,[2,3,5] C. D. MACKAY,[2,15] F. PARESCE,[2,3,5,16] G. WEIGELT,[2,17] D. BAXTER,[3] P. GREENFIELD,[3] R. JEDRZEJEWSKI,[3] A. NOTA,[3,5] S. OSMER,[3] AND W. B. SPARKS[3]

Received 1992 May 26; accepted 1992 July 29

ABSTRACT

Using the Faint Object Camera on-board the *Hubble Space Telescope*, we have obtained images of four planetary nebulae (PNe) in the Magellanic Clouds, namely N2 and N5 in the SMC and N66 and N201 in the LMC. Each nebula was imaged through two narrow-band filters isolating [O III] λ5007 and Hβ, for a nominal exposure time of 1000 s in each filter. Significant detail is evident on the raw images and, after deconvolution using the Richardson-Lucy algorithm, structures as small as 0".06 are easily discernible. In [O III], SMC N5 shows a circular ring structure, with a peak-to-peak diameter of 0".26 and a FWHM of 0".35, while SMC N2 shows an elliptical ring structure with a peak-to-peak diameter of 0".26 × 0".21 (FWHM 0".40 × 0".35). The expansion ages corresponding to the observed structures in SMC N2 and N5 are of the order of 3000 yr. Such low ages appear more easy to reconcile with helium-burning rather than hydrogen-burning central star evolutionary tracks. LMC N201 is very compact, with a FWHM of 0".21 in Hβ. The Type I PN LMC N66 is a multipolar nebula, with the brightest part having an extent of about 2" and with fainter structures extending over 4". The [O III] image reveals structures unprecedented for a planetary nebula, with several bright knots and faint loops visible outside the two main bright lobes.

Subject headings: Magellanic Clouds — planetary nebulae: individual (SMC N2, SMC N5, LMC N66, LMC N201)

1. INTRODUCTION

We have embarked on an imaging survey of Planetary Nebulae (PNe) in the Magellanic Clouds, using the Faint Object Camera (FOC) on-board the *Hubble Space Telescope*. In this *Letter* we present preliminary results on our first four targets, namely N66 and N201 in the Large Magellanic Cloud, and N2 and N5 in the Small Cloud (see Sanduleak, MacConnell, & Philip 1978 for nebular designations). Our pre-launch plan was to obtain both narrow-band optical images and long-slit ultraviolet spectra for a range of PNe. The aberrated telescope optics and the narrowness of the FOC slit (0".1 wide) have forced us to delay spectroscopy until after the first servicing mission. Currently, we are concentrating on FOC optical imaging through the F486N (Hβ) and F501N ([O III]) filters, in combination with existing ground-based and *IUE* spectroscopy, to study these objects.

LMC N201 is the most luminous PN known in [O III] λ5007 and Hβ in the Magellanic Clouds or any other galaxy. Its nebular C/O number ratio is less than unity and its N/O ratio is close to 0.5 (Aller et al. 1987). SMC N2 and N5 have C/O ratios in excess of three (Aller et al. 1987). Ionization structure models of all three nebulae indicate that they are optically thin in the hydrogen Lyman continuum, so that their nebular envelopes are completely ionized (Barlow et al. 1986; Aller et al. 1987). LMC N66 has been classified as a type I PN by Monk, Barlow, & Clegg (1988), on the basis of a high N/O ratio of 0.8. Galactic type I PNe often exhibit pronounced bipolar structures and are believed to originate from the high-mass end of the stellar population that produces planetary nebulae (Peimbert & Torres-Peimbert 1983). Typical sizes of bright planetary nebulae in the Magellanic Clouds are expected to be less than 1", so that even with techniques such as speckle interferometry (Barlow et al. 1986; Wood, Bessel, & Dopita 1986) their diameters are very difficult to measure from the ground. While morphological information can in principle be obtained from high signal-to-noise speckle interferometric data, in practice most results are interpreted in terms of simple structural models, such as uniform disks or edge-brightened rings. Galactic PNe routinely exhibit much more complicated structures than these. On the other hand, Magellanic Cloud

[1] Based on observations with the NASA/ESA *Hubble Space Telescope*, obtained at the Space Telescope Science Institute, which is operated by AURA, Inc., under NASA contract NAS 5-26555.

[2] Member FOC Investigation Definition Team.
[3] Space Telescope Science Institute, 3700 San Martin Drive, Baltimore, MD 21218.
[4] Department of Physics and Astronomy, University College London, Gower Street, London WC1E 6BT, UK.
[5] Affiliated to Astrophysics Division, Space Science Department of ESA.
[6] Space Telescope European Coordinating Facility.
[7] European Southern Observatory, Karl Schwarzschild Strasse 2, D-8046 Garching, Germany.
[8] Osservatorio Astronomico di Padova, Vicolo Osservatorio, 5, I-35122 Padova, Italy.
[9] Royal Greenwich Observatory, Madingley Road, Cambridge CB3 0EZ, UK.
[10] Laboratoire d'Astronomie Spatiale du CNRS, Traverse du Siphon, Les Trois Lucs, F.-13012 Marseille, France.
[11] Department of Physics and Astronomy, University of Wales College of Cardiff, P.O. Box 713, Cardiff CF1 3TH, Wales, UK
[12] Astrophysics Division, Space Science Department of ESA, ESTEC, NL-2200 AG Noordwijk, The Netherlands.
[13] Laboratory for Space Research, Utrecht; Postal address: Space Research Institute, Sorbonnelaan 2, NL-3584 CA Utrecht, The Netherlands.
[14] Astronomy Department, University of California, Berkeley, CA 94720.
[15] Institute of Astronomy, Madingley Road, Cambridge CB3 0HA, UK.
[16] Osservatorio Astronomico di Torino, Strado Osservatorio 20, I-10025, Pino Torinese, Italy.
[17] Max-Planck-Institut für Radioastronomie, Auf dem Hügel 69, D-5300 Bonn 1, Germany.

PN are ideally suited to imaging with the high-resolution f/96 FOC, which has 0".022 square pixels. In this *Letter* we shall show that significantly better values for PN diameters can be obtained by FOC imaging than by previous ground-based attempts, and that their morphological structures are straightforwardly revealed.

2. OBSERVATIONS AND IMAGE ANALYSIS

We imaged each PN through two narrow-band filters, F486N for Hβ λ4861, and F501N for [O III] λ5007, using the f/96 imaging mode of the FOC (Macchetto et al. 1982, 1991). Observing details are given in Table 1. The Hβ line traces emission by the dominant element in the nebula, while [O III] λ5007 is a strong cooling line which traces emission by the dominant O^{++} ion of oxygen. Images in these two lines of well-resolved Galactic PNe, and nebular ionization structure models (e.g., Harrington et al. 1982), show that the O^{++} ion distribution is similar to that of H^+ in most PNe. Our present images also confirm this, but since [O III] λ5007 is typically 5–10 times stronger than Hβ, in this *Letter* we shall concentrate on the observations taken through the F501N filter. The filter predominantly transmits the λ5007 member of the [O III] $\lambda\lambda$4959, 5007 doublet. The systematic radial velocities of the Small and Large Magellanic Clouds shift the [O III] lines by between +2 Å and +5 Å relative to their rest wavelengths. According to the FOC Handbook (Paresce 1990), the F501N filter has a transmission near 68% at the peak wavelength of 5017 Å but below 4965 Å the transmission drops to only a few percent.

We used the 512 × 512 pixel format which has nominally square pixels of 24 μm on a side, corresponding to 0".0224 ($\pm$0".0001) on the sky. Observations were obtained in fine lock. The data were processed through the Institute calibration pipeline which flat fielded and then geometrically corrected the images. Reseaux marks which are fiducial reference marks engraved on the detector face plate were not removed; one mark can be seen near the center of Lobe B in LMC N66 (Fig. 3). We deconvolved the images using a version of the Richardson-Lucy method (Richardson 1972; Lucy 1974) as installed in the IRAF package.

The photon counting detectors of the FOC are susceptible to nonlinearity effects which depend not only on the flux of the source but also on image structure. The aberrated PN images are complex, with both a central bright core and an extensive aberrated halo. Count rates with the F486N Hβ filter are below saturation levels. The F501N [O III] fluxes are higher. LMC N201 is saturated in this filter and would have to be re-observed using neutral density filters. A check of the counts in the other [O III] images give count rates that are below saturation levels.

3. SIZES AND MORPHOLOGIES

The F501N images of SMC N2 and SMC N5 are shown in Figure 1 (Plate L2) and [O III] intensity crosscuts are given in Figure 2. Because the integrated number of counts was conserved during the Richardson-Lucy deconvolutions, the plots in Figure 2 represent the approximate number of counts per pixel that would have been obtained from a nonaberrated telescope. It is ironic to note that in such a case the [O III] images of SMC N2 and N5 would have saturated, with count rates at their peaks on the order of 2–3 counts s^{-1} $pixel^{-1}$.

SMC N2 is a slightly elliptical ringlike nebula, with its greatest elongation in the EW direction. In the deconvolved F501N image the peak-to-peak dimensions of the ring (EW × NS) are 0.26 × 0.21 arcsec^2. The elongation appears more pronounced in the F486N image (not shown), where the peak-to-peak dimensions of the ring are 0.23 × 0.13 arcsec^2. The shape of SMC N5 more closely approximates a circular ring, with the F501N image showing a clearly defined, nearly uniform structure, apart from a brighter patch at the northern edge. The peak-to-peak diameter of the ring is 0".26 and the ring itself is significantly narrower than that of SMC N2, with a width as small as 0".06 (FWHM) in some places.

The deconvolved Hβ image of LMC N201 is Gaussian in shape, with a FWHM of 0".21 (not shown). However, the interpretation of the nebular structure is complicated by the fact that this nebula has a very bright central star, which undoubtedly contributes significantly to the total counts in the F486N filter. Proper allowance for the central star contribution must be made before final conclusions about the nebular structure can be reached. Stellar contamination would be less of a problem in an F501N image since, for LMC N201, [O III] λ5007 is 11 times brighter than Hβ (Monk et al. 1988). However, as mentioned earlier, our F501N image of N201 is saturated.

Figure 3 (Plate L3) shows the F501N image of LMC N66. The identification of the central star is confirmed by the F486N image. Hβ is 9 times weaker than [O III] λ5007 in LMC N66 (Monk et al. 1988) and all of the features seen in the F501N image are proportionately weaker in the F486N image, apart from the peak identified with the central star, which has the same intensity. We have provided the designations in Figure

TABLE 1

FAINT OBJECT CAMERA f/96 OBSERVATIONS OF FOUR PLANETARY NEBULAE IN THE MAGELLANIC CLOUDS

Name	R.A. (J2000)	Decl. (J2000)	Filter	Date (1991 UT)	Exposure (s)	Aperture PA	Max. Count (counts)	Size
SMC N2	$0^h32^m38^s.8$	−71°41′59″	F486N	Jul 9.67	995.9	57°.7	79	0".23 × 0".13 p
			F501N	Jul 9.62	995.9	57.7	440	0.26 × 0.21 p
SMC N5	0 39 26.3	−73 01 42	F486N	Jul 9.82	921.4	56.3	52	0.31 w
			F501N	Jul 9.72	995.9	56.3	411	0.26 p
LMC N66	5 36 20.8	−67 18 08	F486N	Jun 27.00	974.3	338.5	55	complex
			F501N	Jun 26.94	540.3	338.5	70	~4
LMC N201	5 24 55.1	−71 32 56	F486N	Jun 27.87	836.4	339.3	182	0.21 w
			F501N	Jun 27.81	734.3	339.3	>697	saturated

NOTES.—Coordinates from the STScI Guide Star Selection System. The Aperture column gives the Position Angle (PA) of the FOC aperture which is the angle subtended by the detector line direction with respect to North. FOC images have been rotated counterclockwise by the PA values for conventional North (top), East (left) orientation. The size of each planetary is determined from peak to peak measures of the ring (p) or the FWHM (w). The complex morphology of N66 is described in the text and Table 2.

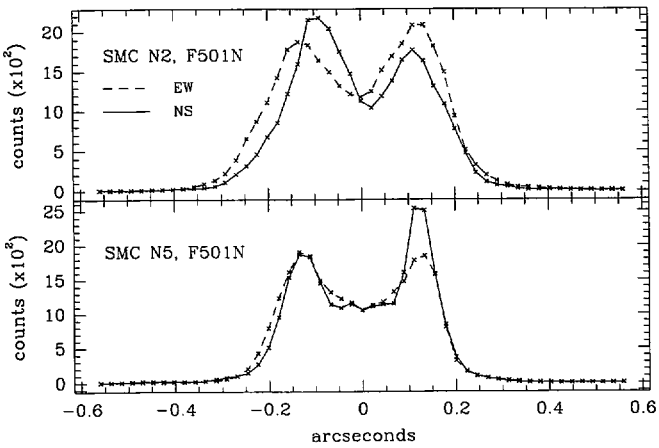

FIG. 2.—Intensity cross-sections through the center of the deconvolved F501N image of SMC N2 (*top*) and N5 (*bottom*) in the east-west and north-south directions. Each cross section is an average of 3 adjacent pixels normal to the scan direction. The intensity scale is in units of FOC counts in the deconvolved image.

3*d*, and in Table 2, to the various morphological features that are discernible on the F501N image of N66. The primary components consist of two lobes extending on either side of the central star along an EW axis. Lobe A has an EW extent of 1".0, while Lobe B has an EW extent of 1".3. Extending from these two main lobes are two faint loops. Loop 1, to the south and east, extends as far as 2".05 from the central star, while Loop 2, to the north and west, extends 2".27. The loops have similar widths, ~0".18. The other important features of the nebular structure are the knots that surround the periphery of the two lobes (Fig. 3*d*). Knot 1 appears to be at one of the bases of Loop 1 and Knot 5 is at one of the bases of Loop 2. Knots 2, 3, and 4 may define another loop, which we tentatively identify as Loop 3. The knots are the smallest resolvable structures in the image, with FWHM widths ranging from 0".27 (Knot 1) to 0".09 (Knot 5).

4. DISCUSSION

Three of the four PNe have been observed from the ground using speckle interferometry. Wood et al. (1986) used autocorrelation and cross-correlation techniques to derive an angular diameter of 0".20 for SMC N2, in agreement with the average peak-to-peak diameter of 0".23 found in the FOC image. Barlow et al. (1986), using an autocorrelation analysis only, fitted their results for SMC N2 with two rings having diameters of 0".44 and 0".76. Standley (1986) used both autocorrelation and cross-correlation techniques to analyze the same data set as Barlow et al. (1986) and obtained a good fit with a single ring model having a peak-to-peak diameter of 0".20. Wood et al. (1986) estimated an angular diameter of greater than 0".5 for LMC N201, compared to the FWHM of 0".21 found here from the F486N image. Matcher (1989) fitted his speckle results for LMC N201 with a ring model having a peak-to-peak diameter of 0".135 (FWHM diameter 0".150). Finally, Wood et al. (1986) derived an angular diameter of 0".32 for LMC N66. Clearly, standard speckle interferometry fails completely when dealing with large and complex structures such as are evident in the F501N image of N66.

TABLE 2

MORPHOLOGY OF LMC N66 IN [O III]

Component Label	Relative Intensity[a]	Position Angle	Distance[b]
Lobe A	37	116	0".50
Lobe B	33	272.5	0.66
Central star	2	0	0
Knot 1	5	162	0.67
Knot 2	3	166	0.12
Knot 3	3	196.5	0.64
Knot 4	1	231	0.94
Knot 5	2	329	0.37
Loop 1	6	155.5	2.05
Loop 2	3	330	2.27
Loop 3	5	228	1.22

[a] Relative intensities have been scaled so they add to 100.

[b] In the case of lobes and knots, the distance in arcsec is measured from the central star to the center of the component, while in the case of the loops the distance is to the furthest point.

In the past, central stars of PNe have been assumed to evolve along hydrogen-shell burning tracks. Such tracks predict a central star age which can be compared with the nebular dynamical expansion age. The latter may be derived from the angular radius of a PN at a known distance if the expansion velocity is known. We consider here the case of SMC N2, but similar conclusions may be drawn for SMC N5, whose expansion velocity (Dopita et al. 1985), spectroscopic characteristics and central star parameters (Aller et al. 1987) are very similar to those of SMC N2. The nebular expansion velocity of SMC N2 is 17 km s^{-1} (Barlow et al. 1986) so, for an adopted distance modulus to the SMC of 18.8, the mean angular radius of 0".11 found here for the ring peak corresponds to an expansion age of 1800 yr if the nebular expansion velocity has been constant since ejection. If, as discussed by Barlow et al. (1986), the nebular expansion velocity has increased linearly with radius since a starting AGB expansion velocity of 10 km s^{-1}, the age of the nebula since ejection would be 2300 yr. These values can be contrasted with the much larger central star evolutionary age of 8000 yr if the $T_{\rm eff}$ = 110,000 K, log g = 5.75 central star (Barlow et al. 1986) is on a Schoenberner (1983) hydrogen-shell burning evolutionary track, corresponding to a central star mass of 0.59 $M_\odot$.

From Figure 2, for both SMC N2 and N5, nebular emission extends out as far as a radius of ~0".25. For a constant expansion velocity of 17 km s^{-1}, this corresponds to an expansion age of 4000 yr (5200 yr if the expansion velocity has increased linearly with radius from a starting value of 10 km s^{-1}). The small nebular expansion age of SMC N2 appears to be more easily reconcilable with the helium-burning evolutionary tracks of Wood & Faulkner (1986), which give a mass of ~0.65 $M_\odot$ and an evolutionary age of 3000 yr for the central star parameters found by Barlow et al. (1986).

The nebular filling factor implied by the diameter and electron density of SMC N2 is of relevance to the above considerations. The angular diameter implies an unphysical filling factor of 30, when used in conjunction with equation (13) of Barlow (1987), along with the [O II] electron density of 3000 cm^{-3} and other nebular parameters listed there. (The ionization structure model of Barlow et al. 1986 for the optically thin nebula SMC N2 indicates that the O^+ responsible for the weak observed [O II] emission is a trace ion originating from recombination of O^{++}, the dominant ion of oxygen in the nebula. As such, the derived [O II] $\lambda\lambda$3726, 3729 density should be representative of conditions in the [O III] emitting region.) In order to reduce the filling factor below unity, the overall nebular

diameter would have to be 3.1 times larger than the peak-to-peak diameter found here. As discussed above, emitting material appears to extend at least as far out as a radius of 0".25, i.e., 2.3 times as far as the ring peak radius. Low surface brightness material may extend well beyond the boundaries of the bright inner ring seen here, analogous to the faint outer shells seen around the bright inner rings of Galactic PNe such as NGC 2392 and NGC3242 (e.g., Chu, Jacoby, & Arendt 1987). Such low surface brightness material could represent a significant fraction of the total nebular mass and account for the filling factor discrepancy described above, while at the same time permitting consistency between the hydrogen-shell burning central star evolutionary age and the nebular expansion age. However, deeper exposures would be needed to reveal such material around SMC N2 and N5.

The F501N image of LMC N66 reveals structures unprecedented for a planetary nebula. Its closest counterpart among Galactic PNe appears to be the type I nebula NGC 6302. The images of NGC 6302 presented by Meaburn & Walsh (1980) show loops and knots similar to those found in LMC N66. However, although some of the structures found in NGC 6302 extend significantly off the main axis defined by its bright lobes, they do so to nothing like the extent shown by Loops 1 and 2 in LMC N66, which are almost orthogonal to the axis defined by the main lobes (Fig. 3*c*). NGC 6302 also resembles LMC N66 in exhibiting multiple discrete high-velocity components, ranging up to ± 150 km s^{-1} about the mean radial velocity in the case of NGC 6302 (Meaburn & Walsh 1980). Dopita et al. (1988) found four discrete velocity components in LMC N66, corresponding to line of sight expansion velocities of ± 46 and ± 68 km s^{-1} about its mean radial velocity. If we assume that the stronger, lower velocity, components correspond to the main lobes of N66 then, for an LMC distance modulus of 18.35, this implies an expansion time scale of ≤ 3000 yr for the centroids of the lobes and up to double this for the lobe extremities. The loop extremities would have the same ages if their expansion velocities are of the order of 100 km s^{-1}. Meaburn & Walsh (1980) interpreted the spatial and velocity structure of NGC 6302 in terms of the wind-produced cavity model of Cantó (1980), in which cavities delineated by shocks form on either side of a wind-producing star located in a dense central disk of material. In the case of NGC 6302 the central star is indeed obscured by a dust disk (Lester & Dinerstein 1984), but the central star of N66 is clearly visible. However, there is an obvious axis nearly devoid of material at a PA of 45° through the central star (Fig. 3*d*) and this may represent the plane of a disk that is now almost dissipated.

We are grateful to Elizabeth Stobie, STScI, for implementation of the Richardson-Lucy deconvolution method in STSDAS/IRAF and assistance with the program. The FOC IDT Support Team, D. Baxter, P. Greenfield, R. Jedrzejewski, and W. B. Sparks, acknowledge support from ESA through contract 6500/85/NL/SK. J. C. Blades, P. Crane, and I. R. King acknowledge support from NASA through contracts NAG5-1733, NAS5-27760 and NAS5-28086, respectively. G. Weigett acknowledges support from the German Space Agency through contract 50 OR 9204.

REFERENCES

Aller, L. H., Keyes, C. D., Maran, S. P., Gull, T. R., Michalitsianos, A. G., & Stecher, T. P. 1987, ApJ, 320, 159
Barlow, M. J. 1987, MNRAS, 227, 161
Barlow, M. J., Morgan, B. L., Standley, C., & Vine, H. 1986, MNRAS, 223, 151
Cantó, J. 1980, A&A, 86, 327
Chu, Y.-H., Jacoby, G. H., & Arendt, R. 1987, ApJS, 64, 529
Dopita, M. A., Ford, H. C., Lawrence, C. J., & Webster, B. L. 1985, ApJ, 296, 390
Dopita, M. A., Meatheringham, S. J., Webster, B. L., & Ford, H. C. 1988, ApJ, 327, 639
Harrington, J. P., Seaton, M. J., Adams, S., & Lutz, J. H. 1982, MNRAS, 199, 517
Lester, D. F., & Dinerstein, H. L. 1984, ApJ, 281, L67
Lucy, L. B. 1974, AJ, 79, 745
Macchetto, F., et al. 1982, in IAU 18th General Assembly, ed. D. N. B. Hall (Greenbelt: NASA), 40
Macchetto, F., et al. 1991, ApJ, 369, L55
Matcher, S. J. 1989, Ph.D. thesis, Univ. London
Meaburn, J., & Walsh, J. R. 1980, MNRAS, 193, 631
Monk, D. J., Barlow, M. J., & Clegg, R. E. S. 1988, MNRAS, 234, 583
Paresce, F. 1990, The Faint Object Camera Instrument Handbook, Version 2.0 (Baltimore: STScI)
Peimbert, M., & Torres-Peimbert, S. 1983, in IAU Symp. 103, Planetary Nebulae, ed. D. R. Flower (Dordrecht: Reidel), 233
Richardson, W. H. 1972, J. Opt. Soc. Am., 62, 55
Sanduleak, N., MacConnell, D. J., & Philip, A. G. D. 1978, PASP, 90, 621
Schoenberner, D. 1983, ApJ, 272, 708
Standley, C. 1986, Ph.D. thesis, Univ. London
Wood, P. R., Bessell, M. S., & Dopita, M. A. 1986, ApJ, 311, 632
Wood, P. R., & Faulkner, D. J. 1986, ApJ, 307, 659

PLATE L2

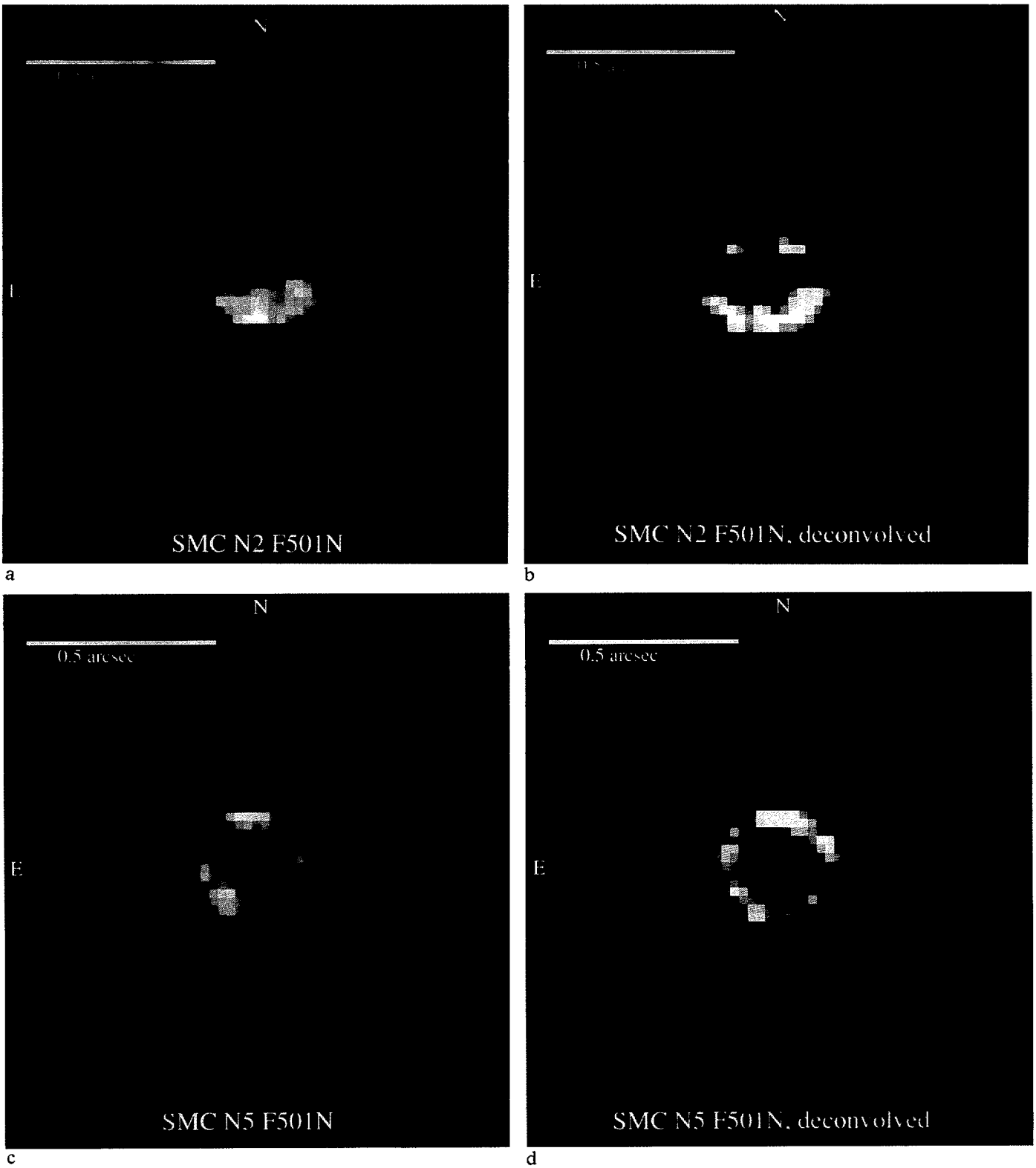

FIG. 1.—*HST* Faint Object Camera images of the SMC PNe, N2 and N5 through the F501N filter. Panels (*a*) and (*c*) show the central regions after calibration but before deconvolution, and panels (*b*) and (*d*) show the images after deconvolution with the Lucy-Richardson method. Each panel is displayed at the same scale and orientation.

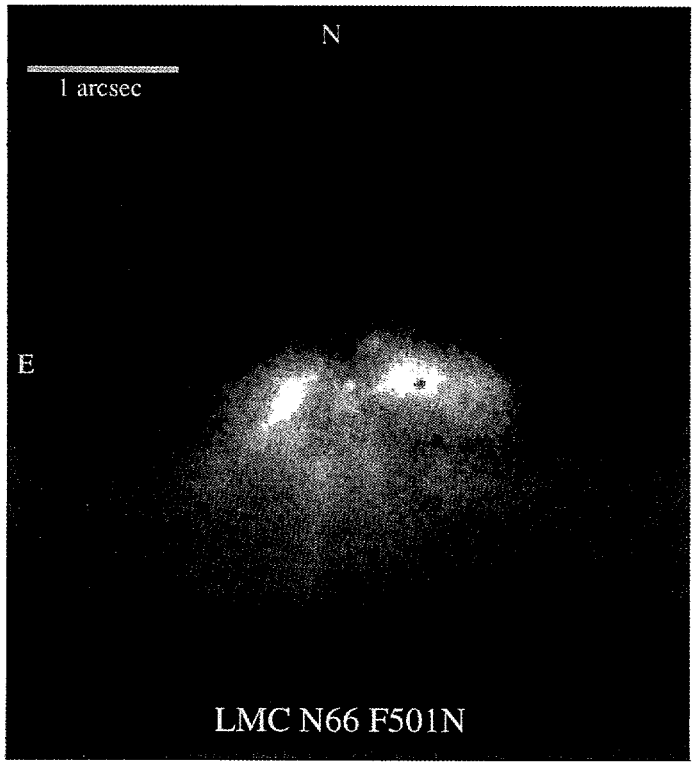

a

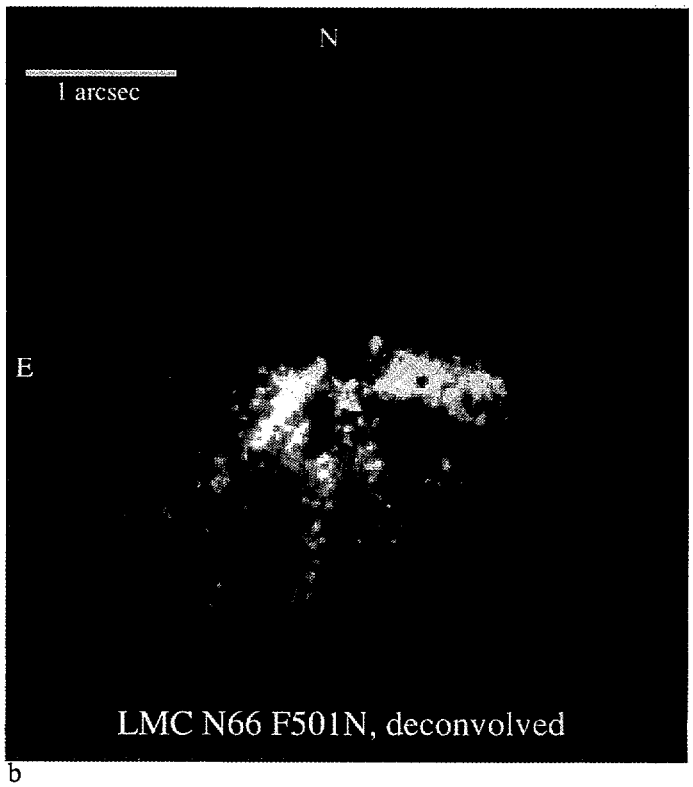

b

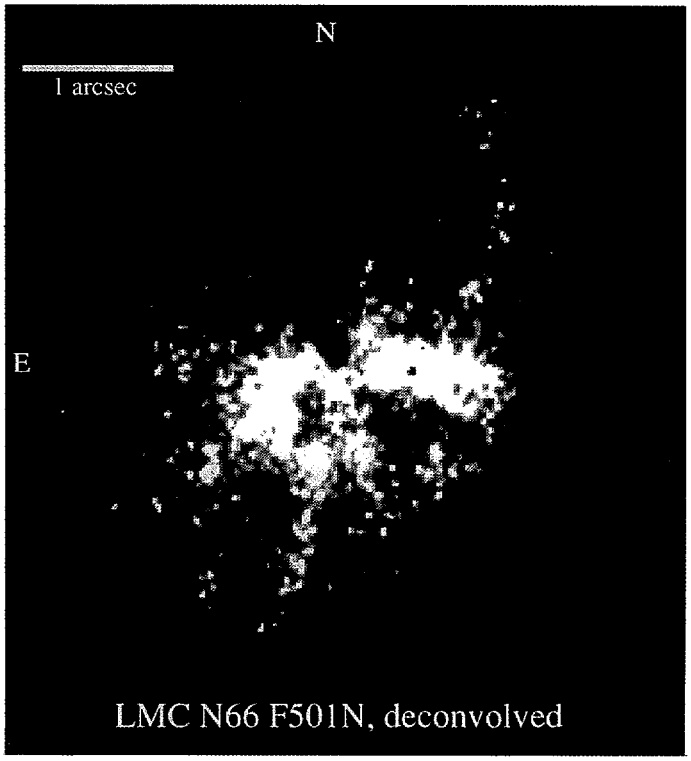

c

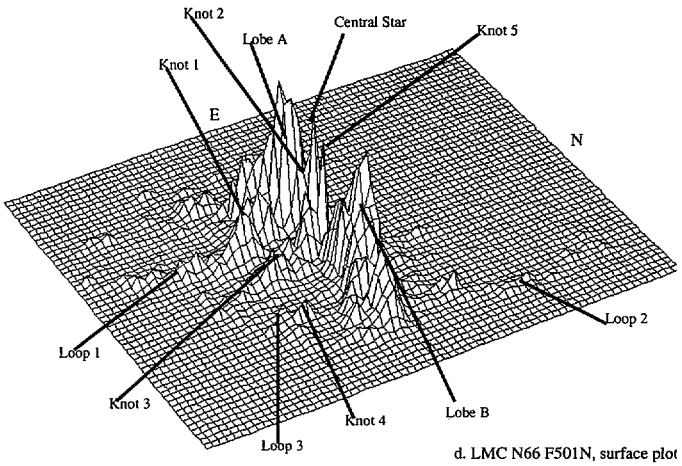

d. LMC N66 F501N, surface plot

FIG. 3.—*HST* Faint Object Camera image of LMC N66 through the F501N filter. Panel (*a*) shows the central part of the image after calibration but before deconvolution. Panel (*b*) shows the image after deconvolution with the Lucy-Richardson method, displayed to show the central star and core; panel (*c*) is a display of the deconvolved image showing the faint nebulosity in the loops. Each panel is displayed at the same scale and orientation. Panel (*d*) is a surface plot of the deconvolved image of the LMC N66 showing the identification of the loops and knots as described in the text and in Table 2.